

# Canted Magnetic Ground State of Quarter-Doped Manganites $R_{0.75}\text{Ca}_{0.25}\text{MnO}_3$ ( $R = \text{Y, Tb, Dy, Ho, and Er}$ )

R. Sinclair,<sup>1</sup> H. B. Cao,<sup>2</sup> V. O. Garlea,<sup>2</sup> M. Lee,<sup>3,4</sup> E. S. Choi,<sup>4</sup>  
Z. L. Dun,<sup>1</sup> S. Dong,<sup>5,\*</sup> E. Dagotto,<sup>1,6</sup> and H. D. Zhou<sup>1,4,†</sup>

<sup>1</sup>*Department of Physics and Astronomy, University of Tennessee, Knoxville, Tennessee 37996-1200, USA*

<sup>2</sup>*Quantum Condensed Matter Division, Oak Ridge National Laboratory, Oak Ridge, Tennessee, 37831, USA*

<sup>3</sup>*Department of Physics, Florida State University, Tallahassee, Florida 32306, USA*

<sup>4</sup>*National High Magnetic Field Laboratory, Florida State University, Tallahassee, Florida 32310, USA*

<sup>5</sup>*Department of Physics, Southeast University, Nanjing 211189, China*

<sup>6</sup>*Materials Science and Technology Division, Oak Ridge National Laboratory, Oak Ridge, Tennessee 37831, USA*

(Dated: March 6, 2022)

Polycrystalline samples of the quarter-doped manganites  $R_{0.75}\text{Ca}_{0.25}\text{MnO}_3$  ( $R = \text{Y, Tb, Dy, Ho, and Er}$ ) were studied by X-ray diffraction and AC/DC susceptibility measurements. All five samples are orthorhombic and exhibit similar magnetic properties: enhanced ferromagnetism below  $T_1$  ( $\sim 80$  K) and a spin glass (SG) state below  $T_{SG}$  ( $\sim 30$  K). With increasing  $R^{3+}$  ionic size, both  $T_1$  and  $T_{SG}$  generally increase. The single crystal neutron diffraction results on  $\text{Tb}_{0.75}\text{Ca}_{0.25}\text{MnO}_3$  revealed that the SG state is mainly composed of a short-range ordered version of a novel canted (i.e. noncollinear) antiferromagnetic spin state. Furthermore, calculations based on the double exchange model for quarter-doped manganites reveal that this new magnetic phase provides a transition state between the ferromagnetic state and the theoretically predicted spin-orthogonal stripe phase.

PACS numbers: 72.80.Ga, 71.30.+h, 75.50.Dd, 61.05.cp

## I. INTRODUCTION

Recent research in the field of manganites has primarily focused on the multiferroic properties of  $\text{RMnO}_3$ .<sup>1-9</sup> This includes studies of Type-I multiferroics employing materials such as the hexagonal  $\text{YMnO}_3$  where ferroelectricity and magnetism have different origins,<sup>10</sup> and also studies of Type-II multiferroics as in the cases of  $\text{TbMnO}_3$  and orthorhombic  $\text{HoMnO}_3$  where the ferroelectricity is caused by peculiar magnetic orders.<sup>11-13</sup> All of these multiferroic  $\text{RMnO}_3$  materials are located in the narrow-bandwidth limit of manganites due to their small  $R^{3+}$  ionic size.<sup>14</sup> The fact that in Type-II multiferroics the ferroelectricity is strongly coupled to magnetism makes it very exciting to explore the possibility of new magnetic states in narrow-bandwidth systems. Discovering exotic magnetic phases may lead to functional multiferroics with high transition temperatures and large spontaneous polarizations.

While the cases of pure undoped manganites have been extensively studied,<sup>15,16</sup> the recent exploration for potential new magnetic phases has focused on doped manganites in the narrow-bandwidth limit.<sup>17,18</sup> The competition between the ferromagnetic double exchange interactions and the antiferromagnetic superexchange interactions, plus the robust Jahn-Teller spin-lattice coupling, makes the doped narrow-bandwidth manganites an ideal playground to search for new magnetic phases.<sup>19</sup> Moreover, considerable theoretical progress has been made in this area of research. For example, the magnetic phase diagram of quarter-doped manganites has been investigated based on the double exchange model.<sup>20</sup> A prominent ferromagnetic (FM) metallic orbitally-disordered phase occupies the region where the superexchange in-

teraction between the  $t_{2g}$  spins,  $J_{\text{AFM}}$ , is small in agreement with the phase diagram of large and intermediate bandwidth manganites. However, a new exotic multiferroic phase, dubbed the spin-orthogonal-stripe (SOS) phase, was found at the large  $J_{\text{AFM}}$  end of the narrow-bandwidth manganites. The SOS state, as shown in Fig. 2(a) of Ref. 20, is made of zigzag chains, as in the CE-phase of manganites at quarter doping, but forming an array of diagonally oriented domains with spins rotated by  $90^\circ$  between domains. Generalizations to other hole dopings have been studied as well.<sup>21</sup>

The intriguing prediction of an SOS state requires detailed experimental studies. Although a couple of previous efforts have been reported for the doped manganites with small  $R^{3+}$  ions, such as  $\text{Tb}_{1-x}\text{Ca}_x\text{MnO}_3$ ,<sup>22-27</sup>  $\text{Dy}_{1-x}\text{Ca}_x\text{MnO}_3$ ,<sup>28</sup> and  $\text{Y}_{1-x}\text{Ca}_x\text{MnO}_3$ ,<sup>29,30</sup> a systematic exploration of quarter-doped manganites  $R_{0.75}\text{Ca}_{0.25}\text{MnO}_3$  has not been conducted and, for this reason, the existence of the SOS phase, or other exotic magnetic phases, has not been confirmed so far. Moreover, theoretically the nature of the quarter-doped manganites with an intermediate  $J_{\text{AFM}}$  strength has not been studied in full detail: it is only known that the FM and SOS states are stable in the limits of small and large  $J_{\text{AFM}}$ , respectively.<sup>20</sup> Thus, an intriguing question develops: does any new magnetic phase exist in the intermediate coupling region in between the FM and the predicted SOS phases? Plenty of previous theoretical studies have consistently shown that manganites in general, i.e. not only multiferroics, have the potential to display a wide variety of complex patterns of spin, charge, and orbital order.<sup>31-35</sup>

With this timely fresh motivation in mind to search for possible new magnetic phases of quarter-doped man-

ganites with a narrow-bandwidth, in this publication we have systematically studied the magnetic characteristics of  $R_{0.75}\text{Ca}_{0.25}\text{MnO}_3$  ( $R = \text{Tb}, \text{Dy}, \text{Ho}, \text{Y}, \text{and Er}$ ). First, we analyzed the magnetic properties of all five polycrystalline samples and found that their general behavior consists of enhanced FM interactions below 80 K and a spin glass state below 30 K. Second, we performed neutron scattering experiments on a single crystal of  $\text{Tb}_{0.75}\text{Ca}_{0.25}\text{MnO}_3$  and discovered that its magnetic ground state is dominated by the short range ordering of a new canted spin state which results in the observed spin glass-like behavior. Finally, we conducted theoretical calculations based on the double exchange model confirming that the observed new spin structure is lower in energy than both the FM and SOS states in the intermediate strength region of  $J_{\text{AFM}}$ ; in other words, the novel magnetic phase reported here acts as a transition state between the FM and the SOS phases.

## II. EXPERIMENTAL DETAILS

Polycrystalline samples of  $R_{0.75}\text{Ca}_{0.25}\text{MnO}_3$  ( $R = \text{Tb}, \text{Dy}, \text{Ho}, \text{Y}, \text{and Er}$ ) were synthesized by solid state reactions. The stoichiometric mixture of  $\text{Tb}_4\text{O}_7/\text{Dy}_2\text{O}_3/\text{Ho}_2\text{O}_3/\text{Y}_2\text{O}_3/\text{Er}_2\text{O}_3$ ,  $\text{CaCO}_3$ , and  $\text{Mn}_2\text{O}_3$  were ground together and then calcined in air at 950 °C, 1200 °C, and 1350 °C for 24 hours, respectively. Single crystals of  $\text{Tb}_{0.75}\text{Ca}_{0.25}\text{MnO}_3$  were grown by the traveling-solvent floating-zone (TSFZ) technique in an IR-heated image furnace (NEC) equipped with two halogen lamps and double ellipsoidal mirrors. The crystal growth rate was 15 mm/h. Small pieces of single crystals were ground into a fine powder for X-ray diffraction. The resulting powder X-ray diffraction (XRD) patterns were recorded at room temperature with a HUBER Imaging Plate Guinier Camera 670 with Ge monochromatized  $\text{Cu } K_{\alpha 1}$  radiation (1.54059 Å). The lattice parameters were refined from the XRD patterns by using the software package *FullProf Suite* with typical refinements for all samples having  $\chi^2 \approx 0.7$ . X-ray Laue diffraction was used to align the crystals. Elastic neutron scattering measurements were performed at the Neutron Powder Diffractometer (HB-2A), and single-crystal neutron scattering measurements were performed at the Four-Circle Diffractometer (HB-3A). Both instruments are located at the High Flux Isotope Reactor (HFIR) in Oak Ridge National Laboratory (ORNL). The neutron scattering diffraction patterns were also refined using *FullProf Suite*. The DC magnetic-susceptibility measurements were performed employing a Quantum Design superconducting interference device (SQUID) magnetometer. The AC susceptibility data was measured on a home-made setup.<sup>36</sup>

## III. RESULTS

### A. Polycrystalline $R_{0.75}\text{Ca}_{0.25}\text{MnO}_3$

Figures 1 (a-e) display the room temperature XRD patterns for  $R_{0.75}\text{Ca}_{0.25}\text{MnO}_3$  ( $R = \text{Tb}, \text{Dy}, \text{Ho}, \text{Y}, \text{and Er}$ ). All samples show a pure orthorhombic ( $Pbnm$ ) structure. With decreasing ionic size  $R$ , the lattice parameters decrease, as shown in Fig. 1(f). The attempts to prepare orthorhombic  $R_{0.75}\text{Ca}_{0.25}\text{MnO}_3$  with  $R^{3+}$  ions smaller than  $\text{Er}^{3+}$  failed. Noting that pure  $\text{HoMnO}_3$ ,  $\text{YMnO}_3$ , and  $\text{ErMnO}_3$  have hexagonal structures, it seems that the substitution of  $\text{Ca}^{2+}$  can stabilize the perovskite structure. This is easy to understand since  $\text{Ca}^{2+}$  ions are larger than the  $R^{3+}$  ions involved here and this doping will reduce the manganese size. Therefore, the structural tolerance factor ( $t$ ) will be increased and, generally, as  $t$  increases the driving force for the octahedral rotation increases as well, leading to the transformation from the hexagonal to the orthorhombic phase. Several reported studies on  $\text{Ho}_{1-x}\text{Ca}_x\text{MnO}_3$  and  $\text{Y}_{1-x}\text{Ca}_x\text{MnO}_3$  have confirmed this observation.<sup>17,30,37</sup>

Figure 2 shows the DC susceptibility ( $\chi$ ) results corresponding to  $R_{0.75}\text{Ca}_{0.25}\text{MnO}_3$ . For the case of  $\text{Tb}_{0.75}\text{Ca}_{0.25}\text{MnO}_3$ ,  $\chi$  shows two major features: (i) a sharp increase around 80 K with decreasing temperature. This feature is more evident as a slope change from the linear temperature dependence of the inverse of the susceptibility (Fig. 2(f)). Here we define the peak position of the derivative of  $1/\chi$  as  $T_1$ . Clearly, ferromagnetic tendencies develop below  $T_1$ ; (ii) a broad peak around 34 K where zero field cooling (ZFC) and field cooling (FC) curves display a large splitting. This peak position is defined as  $T_{SG}$ . Similarly, all other samples also present these two features as well. As shown in Fig. 3, with increasing  $R^{3+}$  ionic size, both  $T_1$  and  $T_{SG}$  generally increase. One important point here is that since  $\text{Y}_{0.75}\text{Ca}_{0.25}\text{MnO}_3$  with nonmagnetic  $\text{Y}^{3+}$  ions display these two features, they must be related to the magnetic  $\text{Mn}^{3+}/\text{Mn}^{4+}$  ions. To further investigate the magnetic properties, we performed a Curie-Weiss fit on the  $1/\chi$  data, as shown in Fig. 2(i), resulting in a Curie temperature of  $\theta_{CW} = 58.1$  K and an effective magnetic moment of  $\mu_{eff} = 5.16 \mu_B$ . For  $\text{Y}_{0.75}\text{Ca}_{0.25}\text{MnO}_3$ , there are 75%  $\text{Mn}^{3+}$  ions ( $\mu_{eff} \approx 4.8 \mu_B$ ) and 25%  $\text{Mn}^{4+}$  ions ( $\mu_{eff} \approx 3.8 \mu_B$ ) in the system, resulting in an expected total effective moment of  $\mu_{eff} \approx 4.6 \mu_B$  which is consistent with our crude fitting analysis.

The AC susceptibility was measured for  $\text{Tb}_{0.75}\text{Ca}_{0.25}\text{MnO}_3$  to study the nature of the transition at  $T_{SG}$ . As shown in Fig. 4(a), around  $T_{SG}$  the AC susceptibility presents a frequency dependent peak. The Mydosh parameter  $\Delta T_{SG}/[T_{SG}\Delta\log(f)]$ , a quantitative measure of the frequency shift, is estimated to be 0.034 (Fig. 4(b)). This is of the same order as the expected range of 0.004-0.018 for conventional spin glass systems.<sup>38</sup> The ZFC and FC splitting feature is also a characteristic behavior of a spin glass transition.

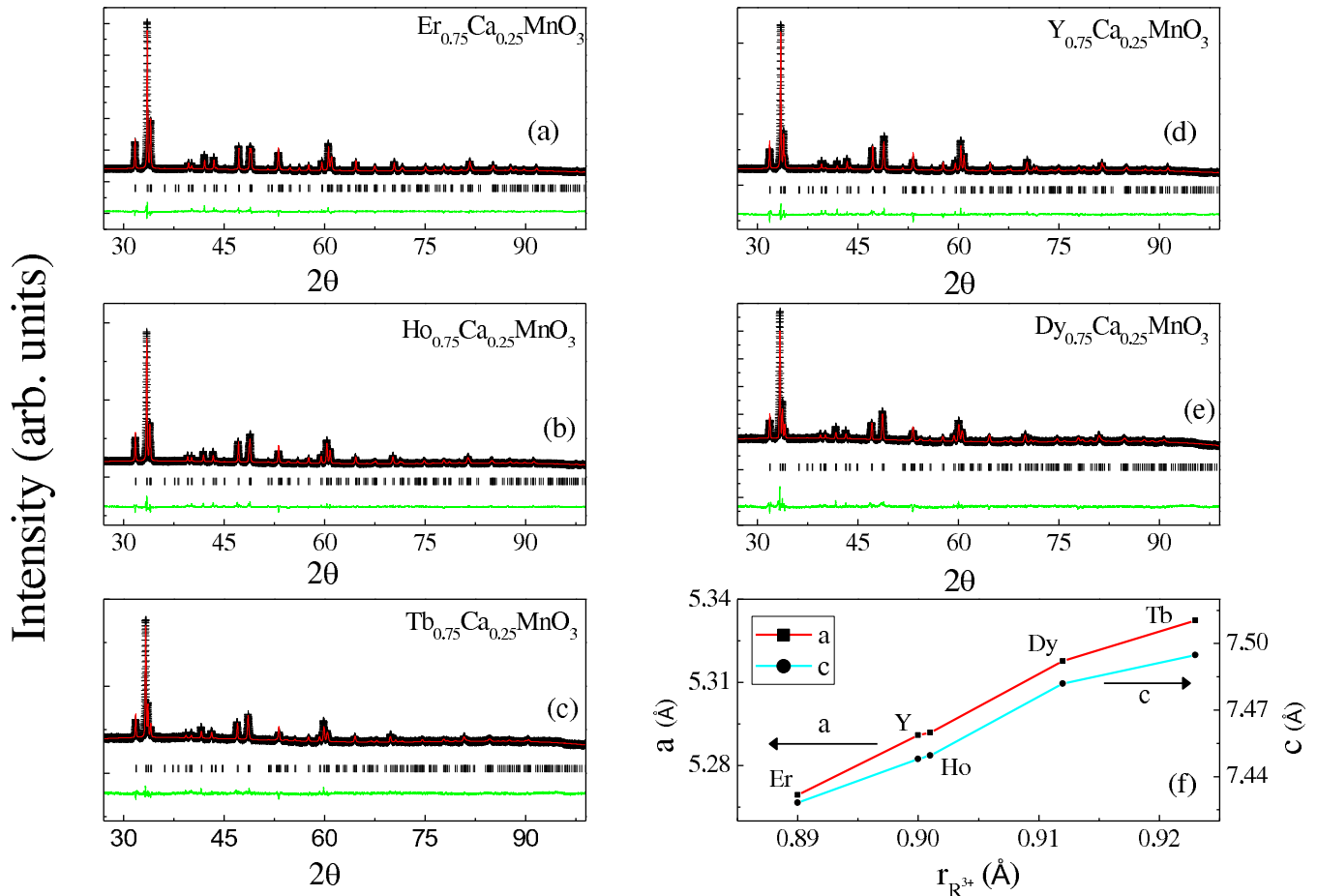


FIG. 1: (color online) Room temperature XRD patterns for polycrystalline  $R_{0.75}Ca_{0.25}MnO_3$ : (a) Er, (b) Ho, (c) Tb, (d) Y, and (e) Dy. The crosses are the experimental data. The solid curves are the best fits from the Rietveld refinement using *FullProf Suite*. The vertical marks indicate the position of the Bragg peaks, and the bottom curves show the difference between the observed and calculated intensities. (f) The  $R^{3+}$  ionic size dependence of the lattice parameters.

The powder neutron diffraction measurements were performed on  $Tb_{0.75}Ca_{0.25}MnO_3$ , and the differential scattering results are shown in Fig. 5. The large feature near  $Q = 2.8 \text{ \AA}^{-1}$  is due to the change in lattice parameters. The negative differential signal at  $Q < 0.5 \text{ \AA}^{-1}$  is caused by the reduction in the paramagnetic scattering that exists above the ordering temperature. Note that the paramagnetic scattering follows the  $Q$  dependence of the  $Mn^{3+}/Mn^{4+}$  magnetic form factor. The observed magnetic peak at  $Q = 1.6 \text{ \AA}^{-1}$  is broader than the instrument resolution. Its position suggests it is due to scattering from a short range ferromagnetic ordering that contributes to the (110) or (002) Bragg peaks which can be explained by a ferromagnetic ordering along either the  $a$  or  $b$  axes. This is consistent with the DC susceptibility results showing the development of ferromagnetism below  $T_1$ . Figure 5(b) contains the differential scattering between 4 K and 120 K. The data shows more pronounced scattering that adds to the (110) or (002) peaks. In addition, there is another new magnetic peak

at  $Q = 1.2 \text{ \AA}^{-1}$ , matching the (100) peak position. The presence of this lattice forbidden (100) peak should be associated with the development of an antiferromagnetic ordering. It is noteworthy that even at 4 K, these peaks are still broader than the instrument resolution, and the correlation length derived from the (100) Lorentzian full peak width at half maximum is approximately  $\xi = 50 \text{ \AA}$ .

Therefore, it is concluded that  $Tb_{0.75}Ca_{0.25}MnO_3$  develops ferromagnetic characteristics below  $T_1$  and enters a short-range ordered state below  $T_{SG}$ , but the latter contains antiferromagnetic tendencies. Based on the similarity among the DC susceptibility measurements of all the  $R_{0.75}Ca_{0.25}MnO_3$  samples, this development of magnetism in the Tb sample should occur in all the other samples as well.

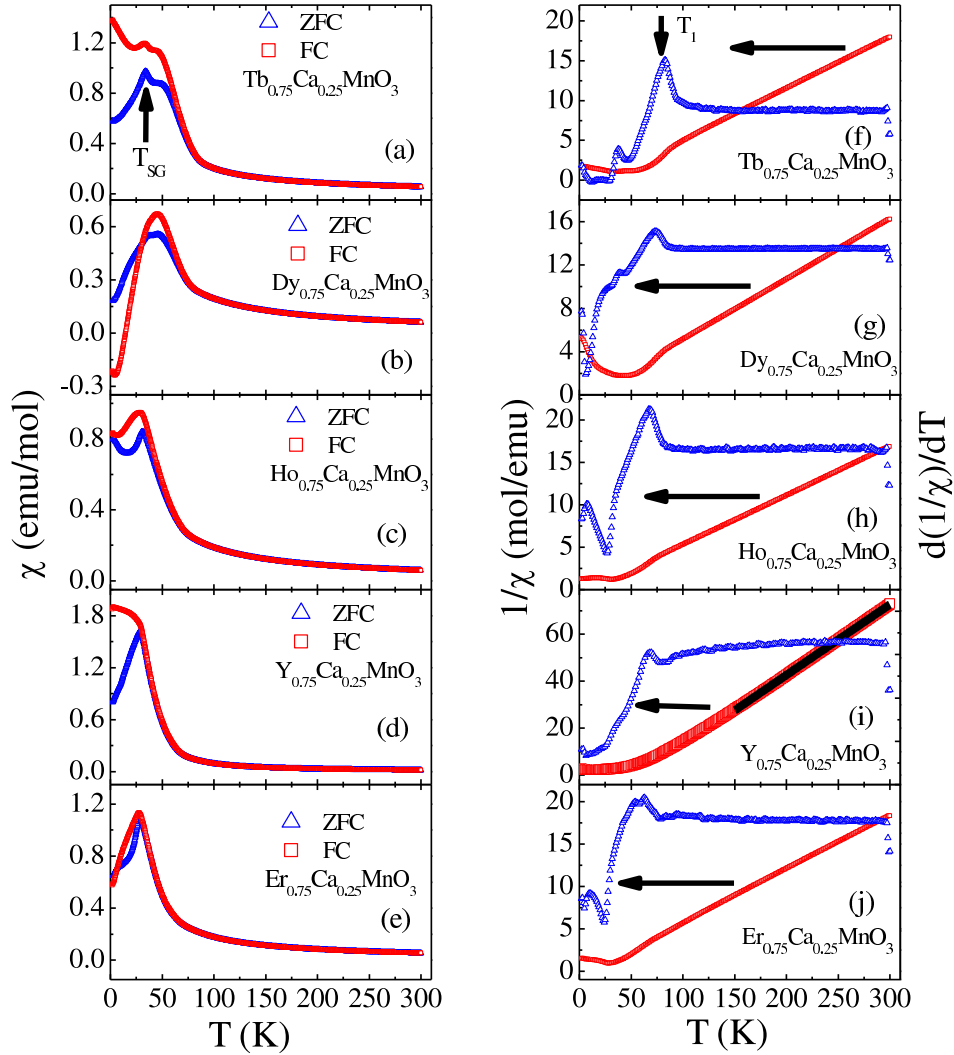


FIG. 2: (color online) Temperature dependence of the DC susceptibility for polycrystalline  $R_{0.75}\text{Ca}_{0.25}\text{MnO}_3$ : (a) Tb, (b) Dy, (c) Ho, (d) Y, and (e) Er. Temperature dependence of the inverse of the susceptibility and its derivative for (f) Tb, (g) Dy, (h) Ho, (i) Y, and (j) Er. In (i), the linear solid line represents the Curie-Weiss fit for the  $T > 150$  K data.

### B. Single crystal $\text{Tb}_{0.75}\text{Ca}_{0.25}\text{MnO}_3$

In order to further clarify the nature of the magnetic properties of  $R_{0.75}\text{Ca}_{0.25}\text{MnO}_3$ , we tried to grow single crystals for more detailed studies. We successfully grew single crystals of  $\text{Tb}_{0.75}\text{Ca}_{0.25}\text{MnO}_3$  by using the floating zone technique. The obtained crystals cleave easily into several millimeter-long needle pieces. The attempts to grow other  $R_{0.75}\text{Ca}_{0.25}\text{MnO}_3$  samples all failed. Notably, after melting at high temperatures, the Ho, Y, and Er samples show phase separation by introducing the hexagonal phase into the orthorhombic phase. This fact suggests that the orthorhombic phase of the Ho, Y, and Er samples is a meta-stable phase at low temperatures. A Laue pattern measured on the grown  $\text{Tb}_{0.75}\text{Ca}_{0.25}\text{MnO}_3$

single crystal is presented in Fig. 6.

Figure 7 shows the DC susceptibility of the  $\text{Tb}_{0.75}\text{Ca}_{0.25}\text{MnO}_3$  single crystal with an applied magnetic field  $H$  along different axes. For  $H||a$  and  $H||c$ , the results for  $\chi$  are similar between the two data sets which shows a slope change around 80 K, as defined by the peak obtained from the derivative of  $1/\chi$ , and a ZFC and FC splitting around 30 K. These features are consistent with the polycrystalline results. For  $H||b$ , the  $\chi$  results are different from those corresponding to  $H||a$  and  $H||c$ . First, the sharp increase of  $\chi$  now shifts to around 50 K. Second, the FC curve keeps increasing below 30 K while the ZFC curve actually shows negative values which strongly suggests the existence of ferromagnetic domains.

As shown in Fig. 8, the single crystal neutron diffraction measurements on  $\text{Tb}_{0.75}\text{Ca}_{0.25}\text{MnO}_3$  display two

TABLE I: Structural parameters for the  $R_{0.75}\text{Ca}_{0.25}\text{MnO}_3$  samples ( $R = \text{Y, Tb, Dy, Ho, and Er}$ ) at room temperature (space group  $Pbnm$ ) determined from refined XRD measurements.

Refinement	Atom	Site	$x$	$y$	$z$	Occupancy
XRD $R = \text{Y}$ $\chi^2 = 0.976$ (a)	Y	4c	-0.01519(29)	0.07107(15)	1/4	0.37365(97)
	Ca	4c	-0.01519(29)	0.07107(15)	1/4	0.12635(97)
	Mn	4b	1/2	0	0	0.50
	O1	4c	0.11811(86)	0.45828(96)	1/4	0.50
	O2	8d	0.69571(76)	0.29496(73)	0.04660(71)	1.00
$a = 5.290982(47), b = 5.626886(54), c = 7.448109(62)$						
Overall B-factor = 1.9561						
XRD $R = \text{Tb}$ $\chi^2 = 0.332$ (b)	Tb	4c	-0.01760(61)	0.06673(33)	1/4	0.37403(133)
	Ca	4c	-0.01760(61)	0.06673(33)	1/4	0.12597(133)
	Mn	4b	1/2	0	0	0.50
	O1	4c	0.09883(233)	0.46518(266)	1/4	0.50
	O2	8d	0.70392(241)	0.29343(216)	0.04061(225)	1.00
$a = 5.333127(126), b = 5.628304(138), c = 7.493484(167)$						
Overall B-factor = 2.4558						
XRD $R = \text{Dy}$ $\chi^2 = 0.697$ (c)	Dy	4c	-0.01432(49)	0.06895(24)	1/4	0.34640(94)
	Ca	4c	-0.01432(49)	0.06895(24)	1/4	0.15360(94)
	Mn	4b	1/2	0	0	0.50
	O1	4c	0.09971(160)	0.47354(181)	1/4	0.50
	O2	8d	0.69111(145)	0.30316(136)	0.04818(147)	1.00
$a = 5.317957(89), b = 5.624245(103), c = 7.482448(124)$						
Overall B-factor = 2.3016						
XRD $R = \text{Ho}$ $\chi^2 = 0.628$ (d)	Ho	4c	-0.01513(31)	0.06859(16)	1/4	0.37244(69)
	Ca	4c	-0.01513(31)	0.06859(16)	1/4	0.12756(69)
	Mn	4b	1/4	0	0	0.50
	O1	4c	0.10984(114)	0.48981(127)	1/4	0.50
	O2	8d	0.70930(115)	0.31137(87)	0.05731(90)	1.00
$a = 5.291904(53), b = 5.640843(58), c = 7.449123(70)$						
Overall B-factor = 2.2878						
XRD $R = \text{Er}$ $\chi^2 = 0.616$ (e)	Er	4c	-0.01729(20)	0.07180(12)	1/4	0.37492(51)
	Ca	4c	-0.01729(20)	0.07180(12)	1/4	0.12508(51)
	Mn	4b	1/4	0	0	0.50
	O1	4c	0.10613(96)	0.46861(103)	1/4	0.50
	O2	8d	0.71026(92)	0.31032(74)	0.05153(64)	1.00
$a = 5.269618(41), b = 5.647665(42), c = 7.428105(54)$						
Overall B-factor = 1.8764						

magnetic signals at low temperatures: (i) a weak broad peak around the antiferromagnetic Bragg position (102); (ii) a strong broad peak around the ferromagnetic Bragg position (002). The temperature dependence of the intensity of the (102) peak shows that it develops below 35 K, which is around  $T_{SG}$ . Meanwhile, the intensity of the shoulder of the (002) peak at  $\theta = 6.5^\circ$  starts developing below 80 K ( $T_1$ ) and sharply increases below 35 K. These features are consistent with the powder neutron diffraction results. The refinement of this single crystal neutron diffraction data leads to the identification of the

magnetic ordering for temperatures lower than 35 K.

The details of the spin structure are shown in Fig. 9. Here, we see that the Mn spins are canted both in and out of the  $a$ - $b$  plane with canting angles of  $\sim 77^\circ$  and  $\sim 32^\circ$ , respectively. The total refined moment of the system was  $3.689 \mu_B$ , as shown in Table II, smaller than our crude Curie-Weiss fit but still robust. This spin structure is different from the canonical A-type, E-type, CE-type, C-type, G-type, and spiral-type antiferromagnetic phases observed in manganites before (using the canonical notation<sup>39,40</sup>). Although the single crystal neu-

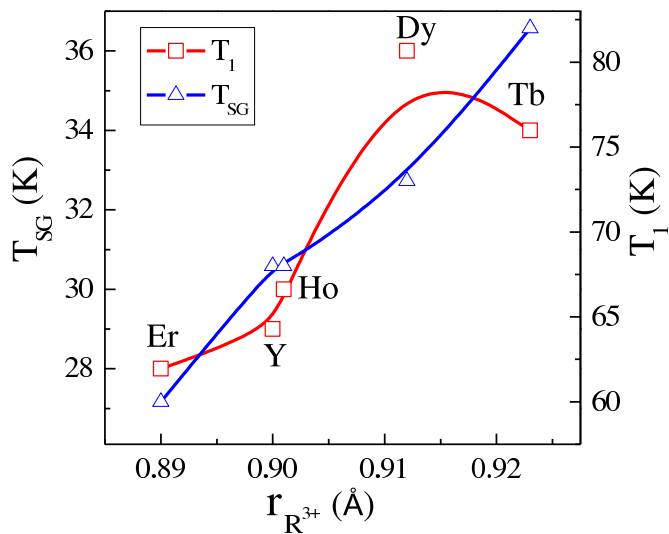


FIG. 3: (color online) Variations of the  $T_1$  and  $T_{SG}$  temperatures with the  $R^{3+}$  ionic size for the  $R_{0.75}\text{Ca}_{0.25}\text{MnO}_3$  materials studied here.

tron data enables us to resolve the antiferromagnetic spin structure, the broadness of the magnetic Bragg peaks strongly suggests that this antiferromagnetic ordering either has short range characteristics or it has a clustered nature, as opposed to a true long range magnetic ordering.

#### IV. DISCUSSION

Only a few previous studies of narrow bandwidth  $R_{1-x}\text{Ca}_x\text{MnO}_3$  have addressed the magnetic properties of  $R_{0.75}\text{Ca}_{0.25}\text{MnO}_3$ .<sup>17,20</sup> For example, Blasco *et al.* analyzed  $\text{Tb}_{1-x}\text{Ca}_x\text{MnO}_3$  and they showed that with increasing Ca doping the ferromagnetic interactions are enhanced while the antiferromagnetic ordering is suppressed, and in particular the  $x = 0.25$  sample has a spin glass ground state.<sup>22</sup> Pena *et al.* focused on  $\text{Dy}_{1-x}\text{Ca}_x\text{MnO}_3$  and they also showed an enhanced ferromagnetic interaction around 80 K for the  $x = 0.25$  sample.<sup>28</sup> In addition, a neutron powder diffraction study of  $\text{Y}_{0.7}\text{Ca}_{0.3}\text{MnO}_3$ , which has a similar composition as the  $\text{Y}_{0.75}\text{Ca}_{0.25}\text{MnO}_3$  case studied here, shows that the magnetic ground state has short range ordering with an antiferromagnetic nature due to the observed broad Bragg magnetic peak around the (001) reflection.<sup>30</sup> Our reported data here is consistent with all of these previous results. More importantly, our systematic studies of  $R_{0.75}\text{Ca}_{0.25}\text{MnO}_3$  point out the presence of enhanced ferromagnetic tendencies around 80 K ( $T_1$ ) and also the existence of spin glass behavior around 30 K ( $T_{SG}$ ). Moreover, these are general behaviors for all  $R_{0.75}\text{Ca}_{0.25}\text{MnO}_3$  with  $R = \text{Tb}, \text{Dy}, \text{Ho}, \text{Y},$  and  $\text{Er}$ . With increasing  $R$  ionic size, both  $T_1$  and  $T_{SG}$  generally increase; in addition, as

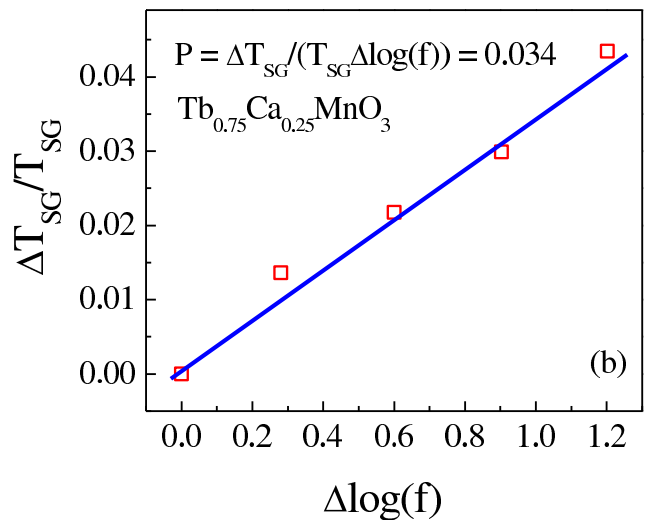
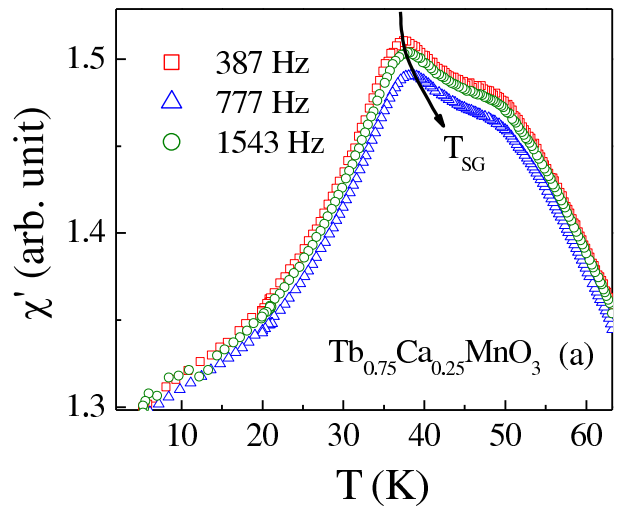


FIG. 4: (color online) (a) Temperature dependence of the real part of the AC susceptibility for polycrystalline  $\text{Tb}_{0.75}\text{Ca}_{0.25}\text{MnO}_3$  under different frequencies. (b) The frequency dependence of  $\Delta T_{SG}/T_{SG}$ .

discussed below the spin glass ground state is compatible with a short range ordering version of a novel canted ferromagnetic spin state that was unveiled based on our detailed neutron diffraction studies on  $\text{Tb}_{0.75}\text{Ca}_{0.25}\text{MnO}_3$  (see Fig. 9).

To verify the exotic magnetic pattern obtained in our neutron analysis, here a microscopic theoretical study is performed based on the standard two-orbital double-exchange model.<sup>39-41</sup> In the past decade, this model Hamiltonian has been widely used to investigate a plethora of magnetic phases and their associated physical characteristics, such as colossal magnetoresistance and multiferroicity, in perovskite manganites.<sup>39,40</sup> The clear success of the previous efforts in this context allows us to investigate with confidence the possibility of new

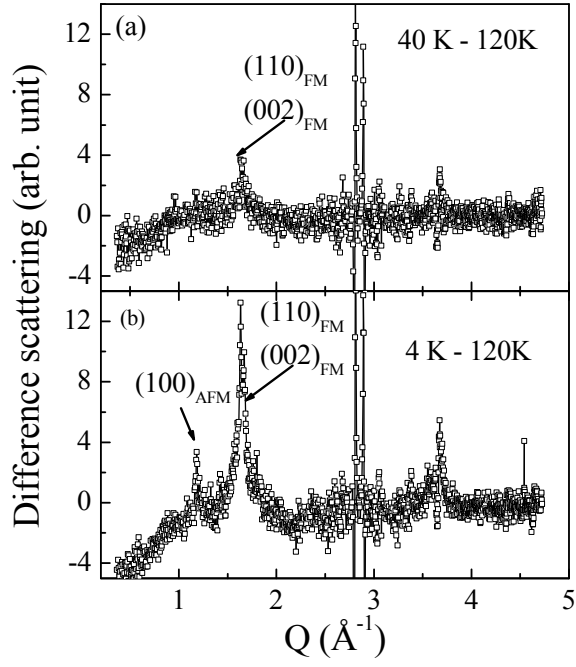


FIG. 5: The differential scattering pattern for polycrystalline  $\text{Tb}_{0.75}\text{Ca}_{0.25}\text{MnO}_3$  (a) between 40 K and 120 K and (b) between 4 K and 120 K.

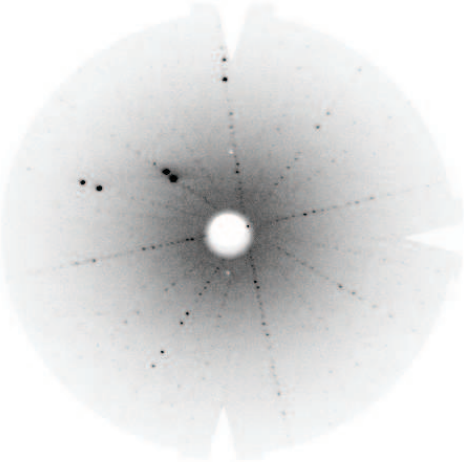


FIG. 6: The Laue pattern oriented along the [001] direction for the grown  $\text{Tb}_{0.75}\text{Ca}_{0.25}\text{MnO}_3$  single crystal.

phases in previously unexplored regions of the phase diagrams via the double exchange model. More explicitly, the model Hamiltonian used here reads as:

$$H = - \sum_{\langle ij \rangle} \sum_{\alpha\beta} t_{\alpha\beta}^{\mathbf{r}} (\Omega_{ij} c_{i,\alpha}^\dagger c_{j,\beta} + h.c.) + J_{\text{AFM}} \sum_{\langle ij \rangle} \mathbf{S}_i \cdot \mathbf{S}_j. \quad (1)$$

This Hamiltonian contains two terms. The first term denotes the standard two-orbital double-exchange hopping process for the  $e_g$  electrons between nearest-

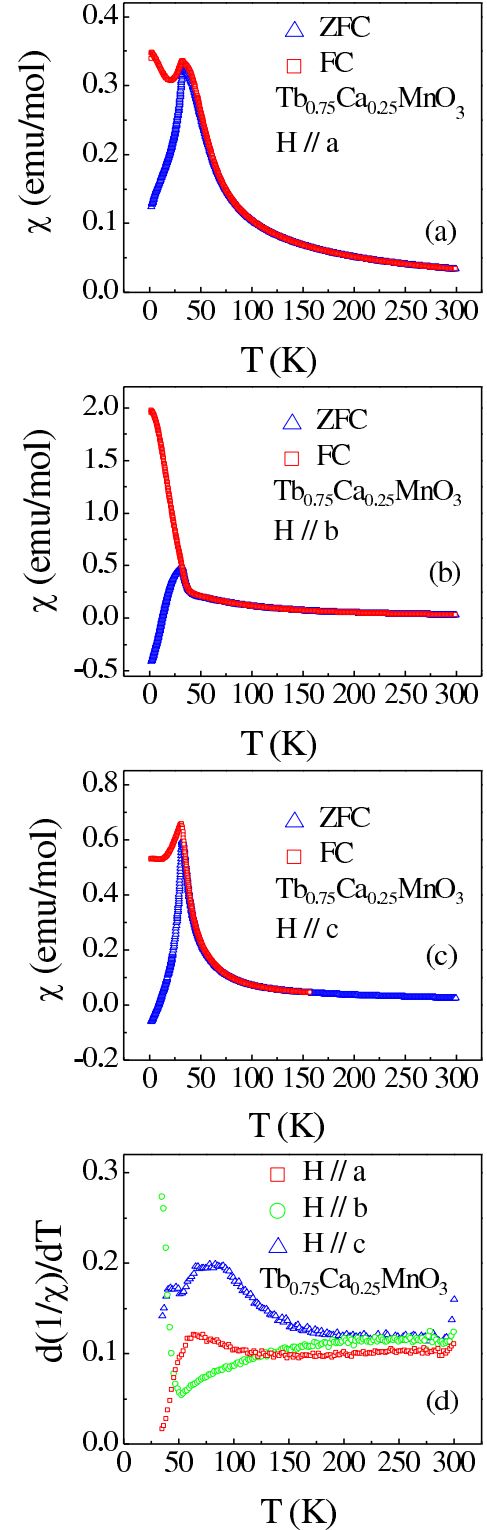


FIG. 7: (color online) Temperature dependence of the DC susceptibility for a single crystal of  $\text{Tb}_{0.75}\text{Ca}_{0.25}\text{MnO}_3$  with (a)  $H||a$ , (b)  $H||b$ , and (c)  $H||c$ . (d) Derivative of  $1/\chi$  with respect to temperature, with  $H$  along the three axes.



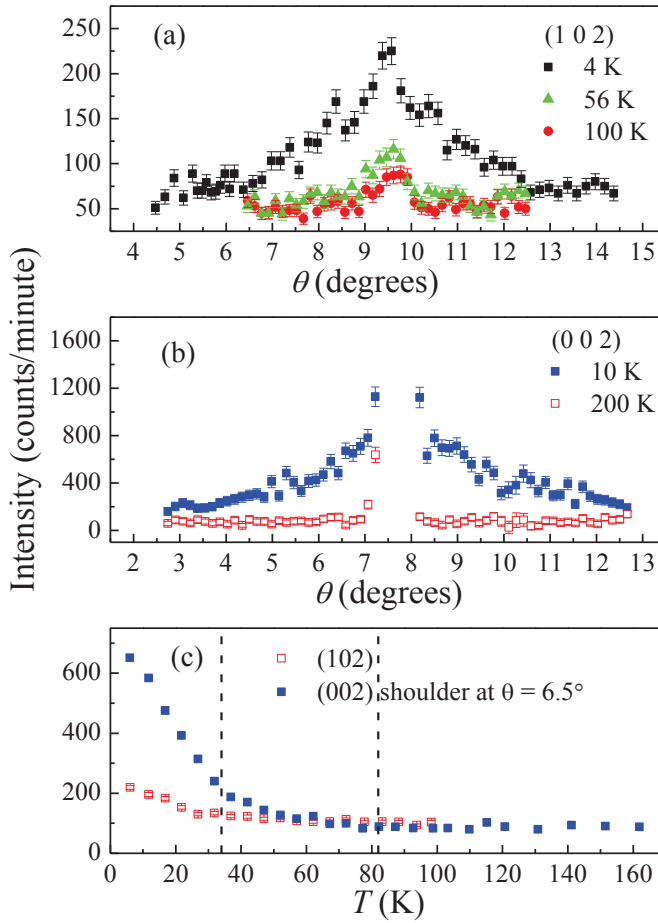


FIG. 8: (color online) The (a) (102) and (b) (002) peaks at different temperatures for the  $\text{Tb}_{0.75}\text{Ca}_{0.25}\text{MnO}_3$  single crystal. (c) Temperature dependence of the (102) peak intensity and the (102) peak shoulder ( $\theta = 6.5^\circ$ ) intensity.

neighbor sites  $i$  and  $j$  of a three dimensional cubic lattice for the manganese ions. The operators  $c_{i,\alpha}^\dagger$  ( $c_{j,\beta}$ ) create (annihilate) an  $e_g$  electron at the orbital  $\alpha$  ( $\beta$ ) of the lattice site  $i$  ( $j$ ). Working within the standard infinite Hund coupling approximation, shown to be qualitatively correct for manganites,<sup>39,40</sup> the spin of the  $e_g$  electrons is always parallel to the spin of the localized  $t_{2g}$  degrees of freedom,  $\mathbf{S}$ , generating the Berry phase:  $\Omega_{ij} = \cos(\theta_i/2) \cos(\theta_j/2) + \sin(\theta_i/2) \sin(\theta_j/2) \exp[-i(\phi_i - \phi_j)]$ , where  $\theta$  and  $\phi$  are the polar and azimuthal angles of the classical  $t_{2g}$  spins, respectively.<sup>39,40</sup> The three nearest-neighbor (NN) hopping directions are denoted by  $\mathbf{r}$ . Two  $e_g$  orbitals ( $a$ :  $x^2 - y^2$  and  $b$ :  $3z^2 - r^2$ ) are involved in the double-exchange process for manganites, with the

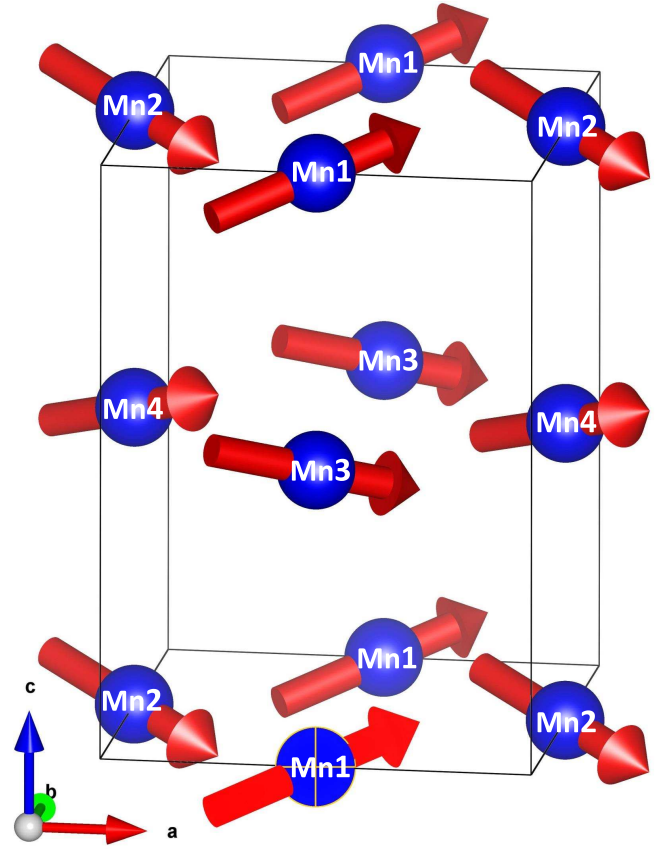


FIG. 9: The novel spin state reported for the  $\text{Tb}_{0.75}\text{Ca}_{0.25}\text{MnO}_3$  lattice. The manganese sites Mn1, Mn2, Mn3, and Mn4 of Table II are indicated. There are two canting angles between Mn's nearest-neighbor spins: an in-plane angle of  $\sim 77^\circ$  and an out-of-plane angle of  $\sim 32^\circ$ .

hopping amplitudes along the three axes given by:

$$\begin{aligned}
 t^x &= \begin{pmatrix} t_{aa}^x & t_{ab}^x \\ t_{ba}^x & t_{bb}^x \end{pmatrix} = \frac{t_0}{4} \begin{pmatrix} 3 & -\sqrt{3} \\ -\sqrt{3} & 1 \end{pmatrix}, \\
 t^y &= \begin{pmatrix} t_{aa}^y & t_{ab}^y \\ t_{ba}^y & t_{bb}^y \end{pmatrix} = \frac{t_0}{4} \begin{pmatrix} 3 & \sqrt{3} \\ \sqrt{3} & 1 \end{pmatrix}, \\
 t^z &= \begin{pmatrix} t_{aa}^z & t_{ab}^z \\ t_{ba}^z & t_{bb}^z \end{pmatrix} = t_0 \begin{pmatrix} 0 & 0 \\ 0 & 1 \end{pmatrix}.
 \end{aligned} \tag{2}$$

In our calculations, the hopping amplitude  $t_0$  will be considered as the unit of energy. This hopping can be roughly estimated to be 0.5 eV.<sup>39,40</sup> The second term of the Hamiltonian is the antiferromagnetic superexchange interaction between the NN  $t_{2g}$  spins.

The typical value of the superexchange coupling  $J_{\text{AFM}}$  in manganites is approximately  $0.1t_0$  for the more widely studied manganites, such as  $\text{La}_{1-x}\text{Sr}_x\text{MnO}_3$  and  $\text{La}_{1-x}\text{Ca}_x\text{MnO}_3$ , based on a variety of previous investigations.<sup>39,40</sup> The model studied here does not include the electron-lattice coupling, i.e. the Jahn-Teller distortions, but this coupling can be partially taken into



TABLE II: Magnetic moments for the single crystal  $\text{Tb}_{0.75}\text{Ca}_{0.25}\text{MnO}_3$  sample at 4.2 K (magnetic space group  $Pbn'm'$ ) determined from refined neutron diffraction measurements.

	x	y	z	$M_x$ ( $\mu_B$ )	$M_y$ ( $\mu_B$ )	$M_z$ ( $\mu_B$ )	M ( $\mu_B$ )
Mn1	1/2	0	0	2.886( 62)	2.063( 75)	1.011(153)	3.6888( 772)
Mn2	0	1/2	0	2.886( 62)	-2.063( 75)	-1.011(153)	3.6888( 772)
Mn3	1/2	0	1/2	2.886( 62)	2.063( 75)	-1.011(153)	3.6888( 772)
Mn4	0	1/2	1/2	2.886( 62)	-2.063( 75)	1.011(153)	3.6888( 772)

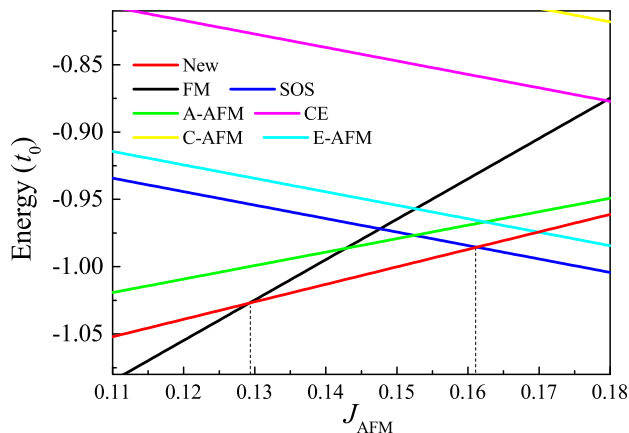


FIG. 10: (color online) Energies (per site) of the magnetic states considered here, as a function of  $J_{\text{AFM}}$ . The energy unit is  $t_0$ . FM: ferromagnetic; A-AFM: A-type antiferromagnetic; C-AFM: C-type antiferromagnetic; E-AFM: E-type antiferromagnetic. These antiferromagnetic as well as the CE labels are standard notations in manganites.<sup>39,40</sup> The SOS state is from Ref. 20. The novel canted state is denoted by “New”.

account by increasing the superexchange strength. Our simplified model is expected to capture the main physics of manganites and, thus, can generate a phase diagram qualitatively similar to the experimental observations.<sup>42</sup> Therefore, it is acceptable to study, at least qualitatively, the properties of the manganites discussed in the present publication using this simplified model.

For the quarter-doped manganites, previous investigations predicted a spin-orthogonal stripe SOS phase in the very narrow bandwidth region ( $J_{\text{AFM}} > 0.17t_0$ ).<sup>20</sup> The well known ferromagnetic phase observed in normal manganites appears in the opposite side ( $J_{\text{AFM}} < 0.13t_0$ ). In the middle region, the Monte Carlo simulation did not provide an unambiguous answer at that time because of metastabilities in the Monte Carlo time evolution that are typically indicative of complex magnetic patterns.<sup>20</sup> Since the spin pattern obtained in the neutron study discussed above is neither the SOS nor the normal ferromagnetic phases, therefore it is necessary to recheck the possible existence of new phases by taking into account the state discovered experimentally here.

The energies for various fixed magnetic patterns are

calculated in momentum space using a fine three dimensional grid and the results are shown in Fig. 10. With increasing  $J_{\text{AFM}}$ , the ground state evolves from the initial ferromagnetic state to the final SOS state, in agreement with previous investigations.<sup>20</sup> However, the most interesting new result is that in the middle region ( $0.129t_0 < J_{\text{AFM}} < 0.161t_0$ ), the newly discovered canted spin order state displays the lowest energy among all of the candidates investigated here.

According to these results, the case of  $\text{Tb}_{0.75}\text{Ca}_{0.25}\text{MnO}_3$  should fall into this middle region. The new canted phase provides a bridge between the ferromagnetic and the SOS phases since it contains both a ferromagnetic and noncollinear components. Thus, the pure SOS phase should be expected to be stable only in even narrower bandwidth manganites.

It is worth clarifying that this canted state does *not* induce ferroelectricity if we apply the inverse Dzyaloshinskii-Moriya (DM) mechanism where lattice distortions leading to ferroelectricity are generated by special noncollinear magnetic states.<sup>11</sup> In the present case the local displacements will compensate between nearest neighbors, and the global ferroelectric polarization will cancel out. Although not ferroelectric, the noncoplanar spin texture of the state unveiled here is very novel, and it can give rise to an intrinsic anomalous Hall effect.<sup>43,44</sup>

## V. CONCLUSIONS

In this publication, we report detailed experimental studies of  $R_{0.75}\text{Ca}_{0.25}\text{MnO}_3$  ( $R = \text{Y, Tb, Dy, Ho, and Er}$ ) polycrystals, and a  $\text{Tb}_{0.75}\text{Ca}_{0.25}\text{MnO}_3$  single crystal, with focus on their magnetic properties. The amount of Ca used corresponds to the hole quarter-doped case of the widely discussed manganite multiferroic perovskites. In general, we have observed the presence of ferromagnetic and spin-glass tendencies in all the samples studied. Our main discovery, using the Tb-based single crystal, is that the spin-glass region appears dominated by the short-range order of a new canted, and thus noncollinear, magnetic state. The theoretical study of the double-exchange model presented here shows that in a reduced region of parameter space the new state has indeed lower energy than the two states previously believed to be dominant at quarter doping in narrow bandwidth manganites, namely the FM and SOS states. The results reported here illustrate that doped manganite multiferroic compounds harbor magnetic states that are more

complex than previously anticipated. Our present efforts are expected to pave the way and motivate more detailed studies of these mainly unexplored exotic materials that have potential for functional applications.

### Acknowledgments

R. S., Z.L.D., and H.D.Z. thank the support from NSF-DMR through Award DMR-1350002. The research at

HFIR/ORNL was sponsored by the Scientific User Facilities Division (H.B.C., O.V.G, J.M.), Office of Basic Energy Sciences, US Department of Energy. S.D. was supported by National Natural Science Foundation of China (Grant Nos. 51322206). E.D. was supported by the National Science Foundation under Grant No. DMR-1404375. The work at NHMFL is supported by Grant No. NSF-DMR-1157490 and the State of Florida and by the additional funding from NHMFL User Collaboration Support Grant.

- 
- \* Electronic address: sdong@seu.edu.cn  
 † Electronic address: hzhou10@utk.edu
- <sup>1</sup> T. Kimura, T. Goto, H. Shintani, K. Ishizaka, T. Arima, and Y. Tokura, *Nature (London)* **426**, 55 (2003).
  - <sup>2</sup> T. Goto, T. Kimura, G. Lawes, A. P. Ramirez, and Y. Tokura, *Phys. Rev. Lett.* **92**, 257201 (2004).
  - <sup>3</sup> M. Kenzelmann, A. B. Harris, S. Jonas, C. Broholm, J. Schefer, S. B. Kim, C. L. Zhang, S.-W. Cheong, O. P. Vajk, and J. W. Lynn, *Phys. Rev. Lett.* **95**, 087206 (2005).
  - <sup>4</sup> T. Kimura, G. Lawes, T. Goto, Y. Tokura, and A. P. Ramirez, *Phys. Rev. B* **71**, 224425 (2005).
  - <sup>5</sup> T. Arima, A. Tokunaga, T. Goto, H. Kimura, Y. Noda, and Y. Tokura, *Phys. Rev. Lett.* **96**, 097202 (2006).
  - <sup>6</sup> M. Mostovoy, *Phys. Rev. Lett.* **96**, 067601 (2006).
  - <sup>7</sup> B. Lorenz, Y. Q. Wang, and C. W. Chu, *Phys. Rev. B* **76**, 104405 (2007).
  - <sup>8</sup> N. Hur, S. Park, P. A. Sharma, J. S. Ahn, S. Guha, and S.-W. Cheong, *Nature (London)* **429**, 392 (2004).
  - <sup>9</sup> L. C. Chapon, G. R. Blake, M. J. Gutmann, S. Park, N. Hur, P. G. Radaelli, and S.-W. Cheong, *Phys. Rev. Lett.* **93**, 177402 (2004).
  - <sup>10</sup> B. B. van Aken, T. T. M. Palstra, A. Filippetti, and N. A. Spaldin, *Nature Mater.* **3**, 164 (2004).
  - <sup>11</sup> I. A. Sergienko and E. Dagotto, *Phys. Rev. B* **73**, 094434 (2006).
  - <sup>12</sup> I. A. Sergienko, C. Şen, and E. Dagotto, *Phys. Rev. Lett.* **97**, 227204 (2006).
  - <sup>13</sup> S. Picozzi, K. Yamauchi, B. Sanyal, I. A. Sergienko, and E. Dagotto, *Phys. Rev. Lett.* **99**, 227201 (2007).
  - <sup>14</sup> A. Maignan, C. Martin, G. Van Tendeloo, M. Hervieu, and B. Raveau, *Phys. Rev. B* **60**, 15214 (1999).
  - <sup>15</sup> S. Ishiwata, Y. Kaneko, Y. Tokunaga, Y. Taguchi, T. Arima, and Y. Tokura, *Phys. Rev. B* **81**, 100411(R) (2010).
  - <sup>16</sup> S. Dong and J.-M. Liu, *Mod. Phys. Lett. B* **26**, 1230004 (2012).
  - <sup>17</sup> N. Jiang, X. Zhang, and Y. Yu, *J. Phys.: Condens. Matter* **25**, 475901(2013).
  - <sup>18</sup> K. Yoshii, H. Abe, and N. Ikeda, *J. Solid State Chem.* **178**, 3615 (2005).
  - <sup>19</sup> S. Demir, I.-R. Jeon, J. R. Long, and T. D. Harris, *Coord. Chem. Rev.* **289-290**, 149 (2015).
  - <sup>20</sup> S. Dong, R. Yu, J.-M. Liu, and E. Dagotto, *Phys. Rev. Lett.* **103**, 107204 (2009).
  - <sup>21</sup> S. Liang, M. Daghofer, S. Dong, C. Şen, and E. Dagotto, *Phys. Rev. B* **84**, 0024408 (2011).
  - <sup>22</sup> J. Blasco, C. Ritter, J. García, J.M. de Teresa, J. Pérez-Cacho, and M.R. Ibarra, *Phys. Rev. B* **62**, 5609 (2000).
  - <sup>23</sup> N. Mufti, A. A. Nugroho, G. R. Blake, and T. T. M. Palstra, *Phys. Rev. B* **78**, 024109 (2008).
  - <sup>24</sup> N. Mufti, G. R. Blake, A. A. Nugroho, and T. T. M. Palstra, *J. Phys.: Condens. Matter* **21**, 452203 (2009).
  - <sup>25</sup> A. Machida, Y. Moritomo, S. Mori, N. Yamamoto, K. Ohoyama, E. Nishibori, M. Takata, M. Sakata, T. Otomo, and A. Nakamura, *J. Phys. Soc. Jpn.* **71**, 27 (2002).
  - <sup>26</sup> A. Machida, Y. Moritomo, K. Ohoyama, and A. Nakamura, *J. Phys. Soc. Jpn.* **70**, 3739 (2001).
  - <sup>27</sup> A. A. Nugroho, Risdiana, N. Mufti, T. T. M. Palstra, I. Watanabe, and M. O. Tjia, *Physica B* **404**, 785 (2009).
  - <sup>28</sup> O. Peña, M. Bahout, D. Gutierrez, P. Duran, and C. Moure, *Solid State Sci.* **5**, 1217 (2003).
  - <sup>29</sup> J. R. Sahu, C. R. Serrao, A. Ghosh, A. Sundaresan, and C. N. R. Rao, *Solid State Commun.* **149**, 49 (2009).
  - <sup>30</sup> M. Dlouhá, S. Vratislav, Z. Jiráček, K. Knížek, and D. Sedmidubský, *Appl. Phys. A: Mater. Sci. Process.* **74**, S673 (2002).
  - <sup>31</sup> T. Hotta, S. Yunoki, M. Mayr, and E. Dagotto, *Phys. Rev. B* **60**, 15009 (1999).
  - <sup>32</sup> T. Hotta, M. Moraghebi, A. Feiguin, A. Moreo, S. Yunoki, and E. Dagotto, *Phys. Rev. Lett.* **90**, 247203 (2003).
  - <sup>33</sup> T. Hotta, A. Feiguin, and E. Dagotto, *Phys. Rev. Lett.* **86**, 4922 (2001).
  - <sup>34</sup> T. Hotta, Y. Takada, H. Koizumi, and E. Dagotto, *Phys. Rev. Lett.* **84**, 2477 (2000).
  - <sup>35</sup> S. Dong, R. Yu, S. Yunoki, J.-M. Liu, and E. Dagotto, *Phys. Rev. B* **78**, 155121 (2008).
  - <sup>36</sup> Z. Dun, X. Li, R. S. Freitas, E. Arrighi, C. R. Dela Cruz, M. Lee, E. S. Choi, H. B. Cao, H. J. Silverstein, C. R. Wiebe, J. G. Cheng, and H. D. Zhou, *Phys. Rev. B* **92**, 024408 (2015).
  - <sup>37</sup> P. P. Rout and B. K. Roul, *J. Mater. Sci.: Mater Electron* **24**, 2493 (2013).
  - <sup>38</sup> J. A. Mydosh *1993 Spin Glasses: An Experimental Introduction* (London: Taylor and Francis).
  - <sup>39</sup> E. Dagotto, *Nanoscale Phase Separation and Colossal Magnetoresistance* (Springer, Berlin, 2002).
  - <sup>40</sup> E. Dagotto, T. Hotta, and A. Moreo, *Phys. Rep.* **344**, 1 (2001).
  - <sup>41</sup> E. Dagotto, J. Burgy, and A. Moreo, *Solid State Communications* **126**, 9 (2003).
  - <sup>42</sup> S. Dong, X. T. Zhang, R. Yu, J.-M. Liu, and E. Dagotto, *Phys. Rev. B* **84**, 155117 (2011).
  - <sup>43</sup> X. Chen, S. Dong, and J.-M. Liu, *Phys. Rev. B* **81**, 064420 (2010).
  - <sup>44</sup> N. Nagaosa, J. Sinova, S. Onoda, A. H. MacDonald, and N. P. Ong, *Rev. Mod. Phys.* **82**, 1539 (2010).